Temperature and density dependence of XANES spectra in warm dense aluminum plasmas

V. Recoules* and S. Mazevet
CEA, DAM, DIF, F-91297 Arpajon, France

(Received 4 May 2009; revised manuscript received 2 July 2009; published 26 August 2009)

Using *ab initio* molecular-dynamics simulations combined with linear-response theory, we calculate the density and temperature dependence of the x-ray absorption near-edge structure (XANES) of a dense aluminum plasma. At solid density and for temperatures increasing up to 6 eV, we see that the XANES spectrum loses its well-known room-temperature structure, first due to melting and second due to loss of correlation in the liquid. Similarly, as the density decreases and the system evolves from a liquid to a plasma, the XANES spectrum becomes less structured. As the density is further lowered and the system turns into an atomic fluid, a pre-edge forms as the $3p$ state becomes bound. We suggest that direct measurements of the XANES spectra in this density region is a unique opportunity to validate pressure ionization models routinely used in plasma physics modeling.

DOI: 10.1103/PhysRevB.80.064110 PACS number(s): 52.50.Jm, 51.30.+i, 51.70.+f, 71.22.+i

The prospect of extending the characterization of dense plasmas and shock compressed matter to near-edge absorption spectroscopy is very appealing both from the theoretical and the experimental sides. X-ray absorption near-edge structure (XANES) refers to the spectral region lying about 40 eV above the absorption edge. X-ray absorption spectroscopy is widely used, for example, in chemistry to identify oxidation degree or in catalysis to identify the geometry of substitution sites. In these situations, the detailed analysis of the XANES spectra brings invaluable information on the electronic structure as well as on the local geometry. Measurements of near-edge absorption spectra of shock compressed matter would potentially bring invaluable information on the evolution of the electronic structure as the system is subject to a significant increase in both pressure and temperature. This was first realized by Bradley *et al.*[1] who performed *K*-edge measurements on shocked chlorine. A significant redshift of the edge was also observed for shock compressed aluminum.[2,3]

From the theoretical side, several attempts have been made to combine electronic structure calculations with plasma models of varying degree of sophistication to provide a description of the near-edge absorption spectra or *K*-edge photoionization position.[4–6] All these models suffer, however, from an inconsistency between the two treatments as these calculations make use of various assumptions to model the electronic or the ionic structures. These two quantities are difficult to obtain, especially in the dense plasma regime where a self-consistent description of the ionic and electronic structures is needed. It is especially true when electron localization-delocalization and/or details of the ionic structure play an important role as, for example, in the nonmetal-metal transition observed, among other systems, in hydrogen,[7] helium,[8] or aluminum.[9]

The use of an *ab initio* electronic structure approach based on density-functional theory combined with molecular-dynamics simulations and linear-response theory has been rather successful at providing, to first order, a satisfying description of this complex state of matter.[10] In addition to the thermodynamical properties, transport properties consistent with the equation of state have been obtained for aluminum in this regime. This includes electrical and thermal conductivities,[9,11,12] absorption coefficient, and Rosseland mean opacities.[13,14] These transport properties have been, however, limited to low frequencies (below 100 eV) due to the use of pseudopotentials.

We recently showed that *ab initio* simulations can be extended to calculate near-edge absorption spectra (XANES) of dense plasmas and shocked compressed matter.[15] This approach provides a first-principle description of both the electronic structure and the thermodynamical state of the system by using large supercells. In the present work, we apply this method to calculate the density and temperature variations in the XANES spectrum of a warm dense aluminum plasma. We consider densities ranging from 0.1 g/cm^3, where the system is an ionized atomic fluid to 7 g/cm^3 where it is a strongly correlated fluid and temperatures ranging from normal conditions, where the system is in a solid state to 5 eV where the liquid turns into a plasma. We find that the dramatic change in the structural properties of the system results in significant variations in the overall XANES spectrum as well as measurable energy shifts due to the increase in density and/or temperature. We further show that the appearance of a pre-edge in the XANES spectrum that can be associated to the metal-nonmetal transition provides a particular rigorous framework to benchmark pressure ionization models routinely used in dense plasma modeling.

I. COMPUTATIONAL METHOD

To simulate aluminum at a given thermodynamic state, we first perform *ab initio* molecular-dynamics simulations using up to 108 atoms initially arranged in an perfect FCC lattice. The initial configuration was propagated up to 1 ps using time steps of 1 fs in the isokinetics ensemble where the velocity are rescaled at every time step to maintain the desired temperature. We used the abinit electronic structure code[16,17] and generated a PAW (projected augmented wave) (Refs. 18 and 19) pseudopotential in the generalized gradient approximation[20] parametrization of density-functional theory using the ATOMPAW generator.[21] The PAW pseudopotential consists in three outer electrons ($3s^2 3p^1$) and a cutoff radius, $r_c = 1.7 a_B$. We used a plane cutoff of 15 Ha and all molecular-

 ©2009 The American Physical Society

dynamics calculations were performed at the Γ point. The adequacy of the pseudopotential generated was checked against all-electron linearized augmented plane waves (LAPW) calculations. For the equilibrium volume and bulk modulus, we obtain, respectively, $V_0=16.98$ Å^3/atm and $K_0=81.59$ GPa which compares well with all-electron calculations, $V_0=16.48$ Å^3/atm and $K_0=75$ GPa.[22]

To obtain the optical response in the x-ray domain, we select equally spaced ionic configurations along the equilibrated part of the trajectory. We then apply linear-response theory as expressed within the Kubo-Greenwood formulation to the ionic configuration at hand.[7,9,13] This formulation leads to the real part of the optical conductivity expressed as

$$\sigma_1(\mathbf{k},\omega)=\frac{2\pi}{3\omega\Omega}\sum_{m=1}^{n_b}\sum_{n=1}^{n_b}[F(\epsilon_{n,\mathbf{k}})-F(\epsilon_{m,\mathbf{k}})]\times|\langle\psi_{m,\mathbf{k}}|\vec{\nabla}|\psi_{n,\mathbf{k}}\rangle|^2\delta(\epsilon_{m,\mathbf{k}}-\epsilon_{n,\mathbf{k}}-\omega). \quad (1)$$

We employ atomic units with the electron charge e, Planck's constant $\hbar$, and the electron mass m_e all set to unity. The n and m summations range over the n_b discrete bands (orbitals) included in the cubic supercell with volume Ω. $F(\epsilon_{n,\mathbf{k}})$ is the Fermi weight corresponding to the energy $\epsilon_{n,\mathbf{k}}$ for the nth band for the **k**-point **k**. The total optical conductivity is obtained by direct summation over all necessary **k** points. In contrast to the molecular-dynamics simulations, this calculation necessitates a detailed electronic structure and **k**-point convergence must be checked.

The electrical and optical properties calculated using Eq. (1) are restricted to photon energies where the outer electrons only participate. As shown in Ref. 15, the method is extended to the calculation of the x-ray absorption spectra by calculating the necessary dipole matrix elements involving core electrons within the PAW following Ref. 23. The PAW matrix elements given by

$$\langle\psi_{m,\mathbf{k}}|\vec{\nabla}|\phi_c\rangle=\langle\tilde{\psi}_{m,\mathbf{k}}|\vec{\nabla}|\phi_c\rangle+\sum_{\mathbf{R},\alpha}\langle\tilde{\psi}_{m,\mathbf{k}}|\tilde{p}_{\mathbf{R},\alpha}\rangle(\langle\phi_{\mathbf{R},\alpha}|\vec{\nabla}|\phi_c\rangle-\langle\tilde{\phi}_{\mathbf{R},\alpha}|\vec{\nabla}|\phi_c\rangle) \quad (2)$$

reduce to

$$\langle\psi_{m,\mathbf{k}}|\vec{\nabla}|\phi_c\rangle=\sum_{\mathbf{R},\alpha}\langle\tilde{\psi}_{m,\mathbf{k}}|\tilde{p}_{\mathbf{R},\alpha}\rangle\langle\phi_{\mathbf{R},\alpha}|\vec{\nabla}|\phi_c\rangle \quad (3)$$

for core electrons whose wave function vanishes outside the PAW sphere of the absorbing atom. This assumes that the pseudopartial wave $|\tilde{\phi}_{\mathbf{R},\alpha}\rangle$ form a complete basis for the pseudowave function $|\tilde{\psi}_{m,\mathbf{k}}\rangle$ within the PAW sphere. We recall that within the PAW formalism, the all-electron wave function, $|\psi_{m,\mathbf{k}}\rangle$, is connected to the pseudowave function, $|\tilde{\psi}_{m,\mathbf{k}}\rangle$, by the relation

$$|\psi_{m,\mathbf{k}}\rangle=|\tilde{\psi}_{m,\mathbf{k}}\rangle+\sum_{\mathbf{R},\alpha}(|\phi_{\mathbf{R},\alpha}\rangle-|\tilde{\phi}_{\mathbf{R},\alpha}\rangle)\langle\tilde{p}_{\mathbf{R},\alpha}|\tilde{\psi}_{m,\mathbf{k}}\rangle. \quad (4)$$

In Eq. (4), **R** represents the sphere, $\Omega_{\mathbf{R}}$, centered on each atomic site. α stands for the angular momentum l, its projection, m, and the principal quantum number, n, used when several projectors are defined. The projectors $|\tilde{p}_{\mathbf{R},\alpha}\rangle$ vanish outside the sphere $\Omega_{\mathbf{R}}$. The partial waves $|\phi_{\mathbf{R},\alpha}\rangle$ and the corresponding pseudopartial wave $|\tilde{\phi}_{\mathbf{R},\alpha}\rangle$ are equal outside $\Omega_{\mathbf{R}}$. We also note that $|\phi_{\mathbf{R},\alpha}\rangle$ form a complete basis in the spheres $\Omega_{\mathbf{R}}$. The core states $|\phi_c\rangle$ are obtained from the all-electron atomic calculation performed when the PAW pseudopotential is generated.

Within single-electron theory, the dominant absorption features of the K-XANES spectrum are described through the excitation of *a* 1*s* electron to the unoccupied (or partially occupied) *p*-like density of states. During the experimental measurements of the XANES spectra, the system is modified by the probe itself as an inner-shell electron is removed.

To take this effect into account, the XANES spectrum is directly obtained using Eq. (3) in the so-called impurity model where the final-state wave function, $|\psi_{m,\mathbf{k}}\rangle$, is determined by considering the absorbing atom in an excited state. This PAW pseudopotential is generated by using a hole in the 1*s* state of the atom while a regular pseudopotential is associated to the other atoms in the supercell. We further point out that this "excited-state" pseudopotential is generated using the same cutoff radius and projectors setting as in the ground-state case. This calculation directly leads to the description of the final state $|\psi_{m,\mathbf{k}}\rangle$ and provides a simple way for introducing the core-electron-hole interaction in the independent-particle description used here.[23,24] We note that within this approximation, the core hole is considered as having an infinite lifetime. The core-hole effect modifies significantly the shape of the spectrum near the absorption threshold and improves the description of the spectrum at 300 K compared to experiment[25] (see Fig. 2 in Ref. 15). This observation is similar to those obtained by Gao *et al.*[26] We further see that the magnitude of the second maximum is also modified. As pointed out previously by Taillefumier *et al.*,[23] this region of the spectrum is, however, rather sensitive to the size of the simulation cell and improvements resulting from the introduction of the electron-hole interaction in this energy region may not hold when using an even bigger simulation cell.

We recall that the absolute position of the *K* edge cannot be formally obtained in the present model. This requires the use of a more sophisticated model based on many-body theory such as a combined GW and Bethe-Salpeter approach. However, this method is computationally to expensive to be applied to the large supercells of interest here.[27]

II. TEMPERATURE DEPENDENCE

In order to investigate the modifications induced by temperature, we carried out calculations of the x-ray absorption spectrum for ten different temperatures ranging from $T=700$ to 60 000 K at solid density. We used a 108 atoms unit cell for the lowest temperatures and reduced the simulation cell to 32 atoms for 30 000 and 60 000 K. All calculations are performed with a $2\times2\times2$ Monkhorst-Pack **k**-point mesh. We carefully tested convergence against calculations using a $3\times3\times3$ grid. Figure 1 shows the effect of the **k**-point mesh for liquid aluminum ($T=60\,000$ K). We see that increasing the number of **k** points above $2\times2\times2$ does not modify the *K* edge position nor the general features of

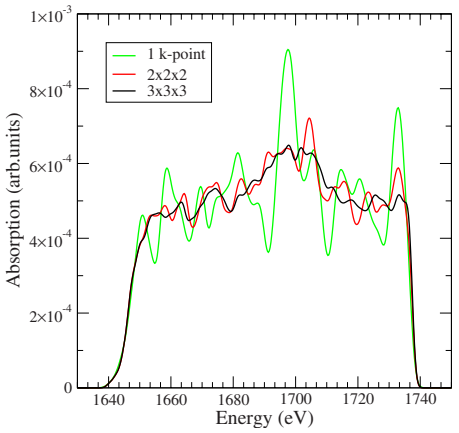

FIG. 1. (Color online) Effect of the k-point mesh for liquid aluminum (T=60 000 K) at ρ_0 density.

the spectra but significantly reduces the smaller oscillations when using an energy broadening of 0.05 hartree.

We show in Fig. 2 the XANES spectra calculated at five different temperatures. The spectra are translated vertically for clarity. We see in Fig. 2 that the spectra exhibit a strong variation in shape as the temperature increases. For T =300 K, the XANES spectra shows two broad absorption peaks and a minimum in the absorption at 1680 eV. The first peak shows two components. This double peaks shape persists as long as the system remains solid. The aluminum melting temperature is 933 K. For temperatures above T =1100 K, the system melts and the two components previously pointed out in the first maximum merge. As the temperature increases further, the entire peak disappears and the minimum at 1680 eV vanishes for temperature higher than T=2000 K. At T=5000 K, we obtain a totally flat spectrum and one can no longer distinguish any particular feature for the disordered system. The XANES spectra formally depend on the local geometry of the atom involved in the x-ray absorption transition and it is useful to consider the pair correlation in this regime. We show in Fig. 3 the evolution of the correlation function as a function of temperature. We

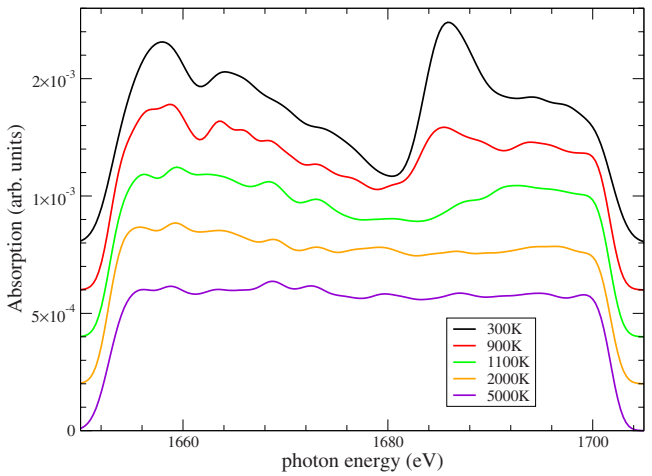

FIG. 2. (Color online) Variation in the XANES spectra in temperature along the ρ_0 isochore.

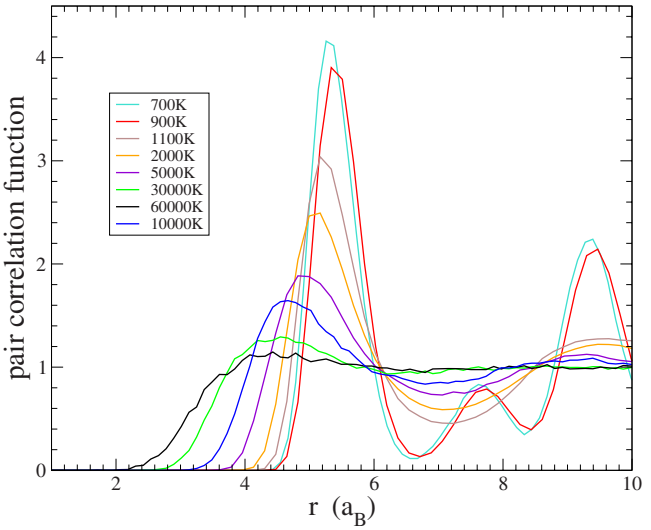

FIG. 3. (Color online) Evolution of radial distribution function as a function of temperature along the ρ_0 isochore.

observe that the disappearance of the second-nearest-neighbor peak can be associated with the disappearance of the double peak structure in the first maximum. This second-nearest-neighbor peak in the correlation function is associated with the fcc state and disappears as soon as the system melts. This analysis suggests that this particular feature of XANES spectra for solid aluminum and its disappearance in the liquid state could be used as a signature for melting. This may not carry over for the minimum at 1680 eV which is still visible in the liquid at T=1100 K. This feature of the XANES spectra appears to be more related to the correlation in the liquid. We do not see however a clear one-to-one correspondence with the degree of correlation as the structure disappears above T=2000 K while the liquid is still correlated with a maximum in the pair-correlation function around $5a_B$.

We now focus on the K-edge shift induced by the increase in temperature. In a fully self-consistent calculation, the 1s orbital energy is affected by the change in density and temperature via the exchange and correlation terms in the Kohn Sham independent-particle equation. This effect is referred to as a chemical shift in surface physics and is routinely used to extract information pertaining to the local environment felt by the atom.[28] In the context of dense plasma calculations, we need to go beyond the frozen-core approximation and introduce the energy variation in the 1s orbital with temperature. In the current work, we estimate the temperature variation in a filled 1s orbital energy by constructing a PAW potential without a core (all electrons are treated as valence electrons) and considering an fcc primitive cell for which the calculation can be performed. The modification of the 1s orbital energy due to the increase in temperature is summarized in Fig. 4. The core-level shift starts to be significant as the temperature reaches 10 000 K. It reaches 0.4 eV at the highest temperature investigated here, T=60 000 K. We also point out that this evaluation is just a first-order estimate of the temperature dependence of the 1s energy. A fully self-consistent calculation within the impurity model would be required to improve on this model. This however requires to

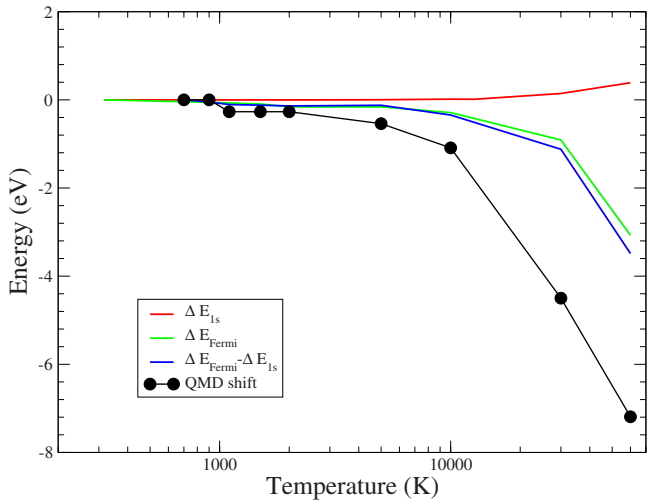

FIG. 4. (Color online) Individual contributions to the K-edge shift along the ρ_0 isochore.

relax the core at each self-consistent cycle and to reevaluate the PAW pseudopotential on the fly. We recall that standard electronic structure calculations use pseudopotentials adjusted on the isolated atom structure. As such, the core density calculated from the frozen-core orbitals are used throughout the calculation. A procedure to relax this constraint and recalculate the pseudopotential consistently was proposed in Ref. 29. The stability of such an algorithm in the context of the impurity model and using large supercells remains to be established. Using the 1s orbital wave functions obtained considering the atom in a ground or excited states, we further found that the 1s wave function and the resulting XANES spectrum are not substantially affected by this energy shift. As such, we thus modified the XANES spectra by introducing the temperature shift of the 1s orbital obtained above.

Figure 5 shows the spectra near the K edge for six different temperatures. As the temperature increases, the K edge is shifted to lower energies. This modification is due to two

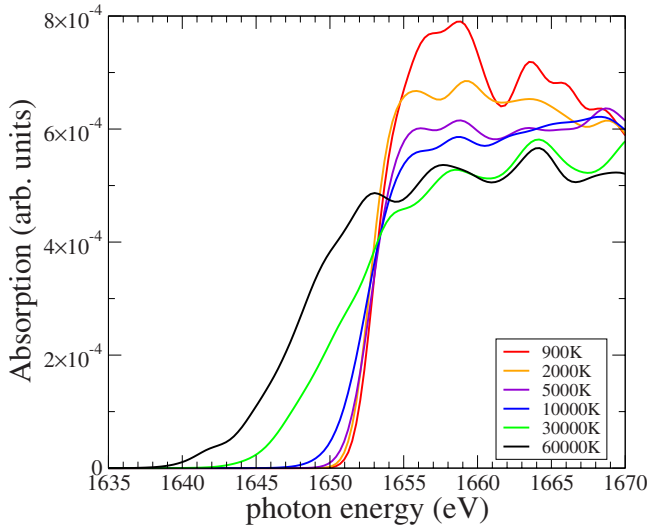

FIG. 5. (Color online) Variation in K edge in temperature along the ρ_0 isochore.

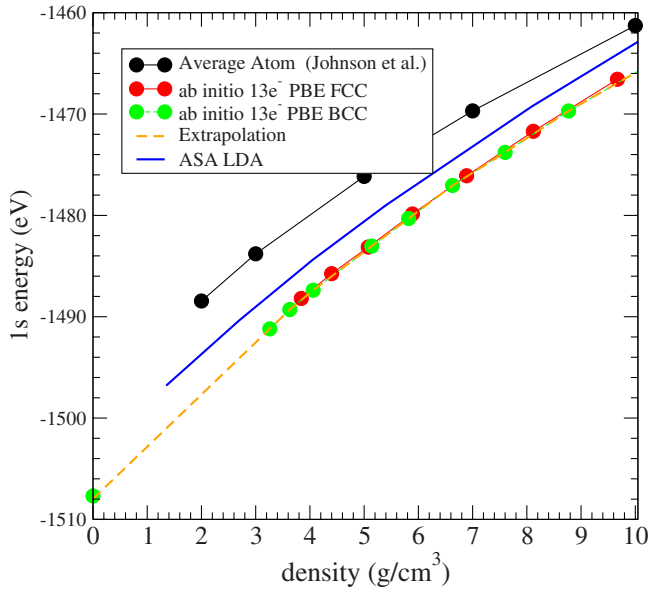

FIG. 6. (Color online) Calculation of the variation in the 1s energy as a function of density.

combined effects. First, the decrease in the Fermi energy by 4 eV when the temperature varies from 300 to 60 000 K and second, the change in population around the Fermi energy. If we defined the K-edge position as an arbitrary value of the absorption coefficient ($\alpha_{\text{threshold}}=1.10^{-4}$ in this case), we find an additional shift of 7 eV coming from the depopulation of states below the Fermi energy. The shape of the edge also reflects this Fermi-Dirac distribution. For $T=900$ K, the edge is sharp similar to the Fermi-Dirac distribution function. Above $T=2000$ K, p-like states start to be depopulated and the K edge moves toward lower energies. As for the Fermi level, this displacement becomes more important when the temperature rises above $T=10\,000$ K. We also point out that the analysis given above could be performed by defining a shift and a broadening as in Ref. 3. We also note that the core-level shift tends to slightly intensify the K-edge shift in Fig. 5 but this effect stays rather weak compared to the two previously quoted.

III. DENSITY DEPENDENCE

To calculate the density dependence of the XANES spectra and K-edge shift, we first evaluate the displacement of the 1s orbital with density. As for temperature, we use the all-electron PAW potential and calculate the variation in the 1s orbital energy for different crystallographic structures. For the calculations shown in Fig. 6, the size of the primitive unit cell drives the density while the temperature is kept at zero. We see in Fig. 6 that we find no significant dependence of the 1s orbital energy on the ionic structure used. We further see that contrary to what was found above, the 1s orbital energy is now significantly shifted by about 40 eV when the density varies up to 10 g/cm^3. The energy shift of the 1s orbital found using the all-electron PAW pseudopotential is also in agreement with calculations performed using an average atom model[30] or with the all-electron LAPW

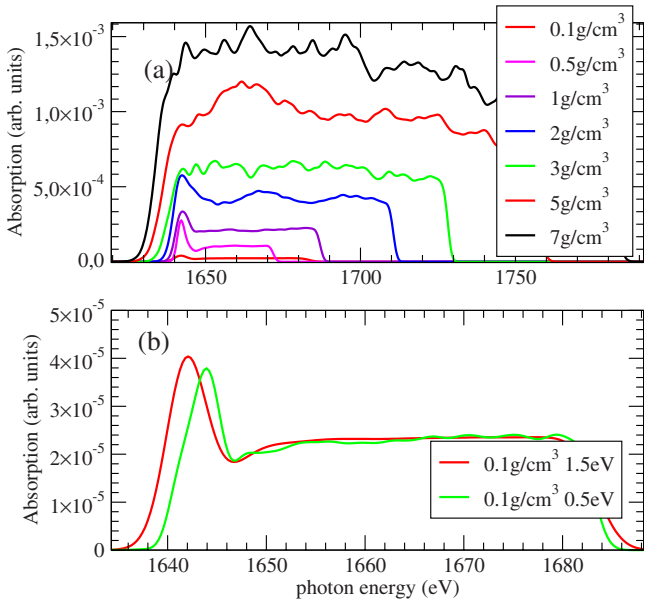

FIG. 7. (Color online) Variation in the XANES spectra in density along the 1.5 eV isotherm.

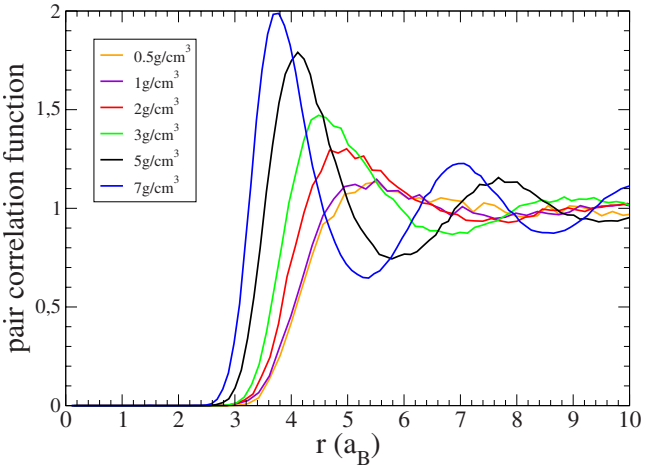

FIG. 8. (Color online) Variation in the pair-correlation function as a function of density.

calculations.[22] As an all-electron method, the latter provides the exact displacement of the $1s$ orbital energy with density. The average atom model is routinely used to calculate the equation of state of dense plasmas and determines, at a given density and temperature, the atomic states occurring within the Wigner-Seitz sphere. The agreement with the all-electron pseudopotential calculations is further evidence that the shift of the $1s$ energy is driven by the increase in density only, with little dependence on the crystallographic structure at hand. We further see in Fig. 6 that this variation is almost linear and can be linearly extrapolated to the isolated atom value.

We now turn to the effect of density on the XANES spectra. We carried out calculations of the absorption spectra for seven densities ranging from $\rho=0.1$ g/cm^3 to $\rho=7$ g/cc along the 1.5 eV isotherm ($T=17\,400$ K). We used 54 atoms in the unit cell and performed all the calculations using, as before, a $2\times2\times2$ Monkhorst-Pack **k**-point mesh. Figure 7 shows the resulting x-ray spectra corrected at each density by the energy of the $1s$ orbital. For all the densities studied, aluminum is liquid and the system becomes more and more structured as the density increases. Figure 8 shows the evolution of the pair-correlation function as a function of density. At this elevated temperature, we find that there exists almost no significant structure in the XANES spectrum as the systems becomes more structured when the density increases from normal conditions and up to 7 g/cm^3.

At these densities, the most significant change along the 1.5 eV isotherm is reflected in the edge displacement. The edge moves toward lower energies due to the competing effect of the increase in both the Fermi energy and the $1s$ orbital energy. As before, we further stress that we only approximate this effect and that a fully self-consistent calculation would be required to describe the displacement from an *ab initio* stand point. We further note that a direct measurement of the *K*-edge position would provide a stringent test for *ab initio* methods based on pseudopotentials and their accuracy at high densities. While it is likely that the core density is not significantly affected by the energy displacement of the $1s$ orbital, a quantification of this uncertainty on the resulting equation of state and optical properties for dense plasmas (where all-electron approaches cannot be easily employed) is necessary.

When the density is lowered to 0.1 g/cm^3, a pre-edge peak appears. As shown previously,[9,11,13] the ionization fraction of the system varies from three to one as the density is reduced from normal conditions down to 0.1 g/cm^3. The system thus evolves from having three electrons in the conduction band due to the effect of density to a single electron due, this time, to the effect of temperature. This effect is also known as pressure ionization. A calculation of the absorption coefficient at the same density (given in Ref. 13) shows an atomic transition that can be identified to the $3s\rightarrow3p$ transition of the singly ionized ion at the lowest density.

We see in Fig. 7(a) that the appearance of the $1s\rightarrow3p$ transition translates into the formation of a pre-edge structure in the XANES spectra at the lowest density. We also see that the formation of the pre-edge peak can be anticipated as soon as 2 g/cm^3 by the formation of a maximum near the edge. This indicates that the metallic electrons lose their free-electronlike characteristic as soon as the density is lowered below normal density. As the XANES spectrum is proportional to the p component of the projected density of states around the absorbing atom, this shows that measurements in this regime provide a framework not only to test pressure ionization models but also to provide detailed information on the changes occurring in the electronic structure as the system evolves from a simple atomic systems to a dense plasma. We show in Fig. 7(b), the XANES spectra at the lowest density and two different temperatures, $T=0.5$ and 1.5 eV (respectively, 5802 and 17 406 K). For both temperatures, the pre-edge identified as a $1s\rightarrow3p$ like transition is clearly visible. This suggests that the effect of the varying density on the electronic structure could be captured experimentally over a rather large temperature range as was the case for the electrical conductivity measurements.[11]

TABLE I. Computed temperature, pressure, and density of aluminum along the principal Hugoniot.

T (K)	P (GPa)	ρ (g cm^3)
900	50	3.5
2500	100	4.0
9863	250	5.0
28313	550	6.0
42470	750	6.5
61617	950	7.0

IV. HUGONIOT

As measurements of the K-edge shift have been made close to the aluminum Hugoniot,[3] we performed molecular-dynamics simulations at temperatures and densities given in Table I that match the SESAME principal Hugoniot.[31] The SESAME table 3700 provides a good description of aluminum at the conditions described here.[32] These simulations are performed far enough from the melting point to reproduce accurately the state of the system with a liquid at and above 5 g/cm^3 and a heated fcc solid below this density. The Hugoniot crosses the high-pressure melting line around 4.5 g/cm^3 ($T_m \sim 4700$ K at $P=132$ GPa). Table I details the thermodynamic conditions simulated. The *ab initio* spectra along the Hugoniot have already been given in Ref. 15 where we obtained a structured spectra in the solid and a rather smooth x-ray absorption in the liquid as shown above. Figure 9 shows the variation in the K-edge shift along the Hugoniot and a comparison with the experimental results of Refs. 2 and 3. As previously, the K-edge position is defined as a threshold value of the absorption coefficient ($\alpha_{\text{threshold}} = 1 \times 10^{-4}$). In contrast to the result given previously,[15] we have accounted for the variation in the 1s orbital energy with both density and temperature by using the results of the previous sections. We point out that the temperature correction to the 1s orbital remains very moderate and only reaches 0.4 eV at the highest temperature. As the temperature correction is not consistently obtained with the density correction, we included the latter as an error bar in the final shift given by the size of the points in the figures.

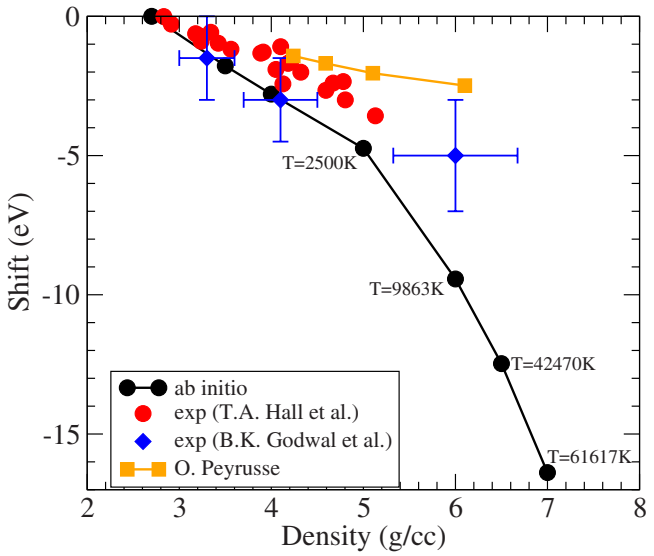

FIG. 9. (Color online) Comparison of the K-edge shift with the experimental measurements (Refs. 3 and 5).

As we move along the Hugoniot, the K edge is shifted toward lower frequencies. This variation is the result of several competing effects. Up to 5 g/cm^3, the K-edge shift is mostly due to density and stays below 5 eV. As the density increases, the energy of the 1s orbital rises by 10 eV while the Fermi level increases by 6 eV. We show in Fig. 9 a direct comparison with the measurements. We find that the calculated K-edge shift compares well with both sets of experimental data. We further note that the measurements were not performed exactly along the principal Hugoniot and are actually reported to be at almost constant temperature ($T = 1.5$ eV) for Ref. 3. We further notice that the good agreement with the experimental data may be improved by the fact that there is no significant broadening due to the temperature which remains below 10 000 K in this density regime. These measurements thus provide a useful validation of the approach at describing density effect for these low-temperature conditions.

For densities above 5 g/cm^3, the temperature along the Hugoniot rises to 61 617 K. The K-edge shift sharply increases to reach a value of 16 eV at the highest point investigated along the Hugoniot. Here, the shift is now due to the combined effect of both temperature and density. At 7 g/cm^3 and $T=61\,000$ K, the shift induced by the variation in the Fermi energy and 1s orbital is around 7 eV. The remaining 9 eV arise from the broadening of the K-edge due to the depopulation of the levels below the Fermi energy. The comparison with the experimental point obtained at a density of $\rho=6$ g cm^3 indicates that the calculated shift may be overestimated at these conditions. We note, however, that the definition of the edge comes into play as soon as the temperature is significant.

This also partially explains the discrepancies with the variation in the magnitude of the K-edge recently predicted by a model based on an averaged-atom calculation combined with the explicit determination of the XANES spectra in real space. We see in Fig. 9 that this model predicts a smaller K-edge variation along the Hugoniot as the current calculation. A direct comparison of the overall XANES spectra further shows that the definition of the K edge alone does not explain the discrepancies and significant differences with the current calculation in the evolution of the XANES spectra along the Hugoniot can be found. Moreover, the author uses the Slater's transition state method to evaluate the 1s energy orbitals.[6] The density effect on this energy orbitals is less pronounced in this case. While the calculation presented here provides a consistent description of the plasma state and the x-ray response, the lack of agreement with the experimental data at this highest density calls for further measurements along the shock compressed Hugoniot. This would allow to access and validate the calculation of the effect of both the temperature and densities on the XANES spectrum and the associated K edge.

V. CONCLUSION

In summary, we calculated the XANES absorption spectra and *K*-edge shift of dense plasmas based on first-principle electronic structure calculations and molecular-dynamics simulations. We used the impurity model by introducing an impurity in the supercell with a PAW atomic data generated with a hole in the 1*s* shell. We showed that calculations of the *K*-edge shift require going beyond the frozen-core approximation and provide a stringent test for the accuracy of pseudopotential-based methods at describing matter under extreme conditions of temperature and density.

We carefully analyzed the variations in the XANES spectrum as a function of increasing density and temperature. For aluminum, we found that some structure in the first maximum near the edge may be used to quantify the solid-liquid phase transition which may prove difficult to identify with current experimental accuracy. While the disappearance of the second maximum of the XANES spectrum is related to the loss of correlation in the liquid, there is no one-to-one correspondence between the two. Finally, we found that the transition from a dense plasma to an ionized atomic fluid is related to the formation of a pre-edge. Measurements in this temperature-density domain would provide stringent test to current modeling of pressure ionization in dense plasmas.

ACKNOWLEDGMENTS

The authors wish to acknowledge useful discussions with P. Renaudin, F. Dorchies, J. Fuchs, O. Peyrusse, and A. Ng, as well as M. Torrent for his precious help with the ABINIT code.

*vanina.recoules@cea.fr

[1] D. K. Bradley, J. Kilkenny, S. J. Rose, and J. D. Hares, Phys. Rev. Lett. **59**, 2995 (1987).
[2] L. DaSilva, A. Ng, B. K. Godwal, G. Chiu, F. Cottet, M. C. Richardson, P. A. Jaanimagi, and Y. T. Lee, Phys. Rev. Lett. **62**, 1623 (1989).
[3] T. A. Hall, J. Al-Kuzee, A. Benuzzi, M. Koenig, J. Krishnan, N. Grandjouan, D. Batani, S. Bossi, and S. Nicolella, Europhys. Lett. **41**, 495 (1998).
[4] F. Perrot and M. W. C. Dharma-wardana, Phys. Rev. Lett. **71**, 797 (1993).
[5] B. K. Godwal, A. Ng, L. DaSilva, Y. T. Lee, and D. A. Liberman, Phys. Rev. A **40**, 4521 (1989).
[6] O. Peyrusse, J. Phys.: Condens. Matter **20**, 195211 (2008).
[7] L. A. Collins, S. R. Bickham, J. D. Kress, S. Mazevet, T. J. Lenosky, N. J. Troullier, and W. Windl, Phys. Rev. B **63**, 184110 (2001).
[8] P. M. Kowalski, S. Mazevet, D. Saumon, and M. Challacombe, Phys. Rev. B **76**, 075112 (2007).
[9] M. P. Desjarlais, J. D. Kress, and L. A. Collins, Phys. Rev. E **66**, 025401(R) (2002).
[10] S. Mazevet, J. Kress, and L. A. Collins, in *Atomic Processes in Plasmas*, AIP Conf. Proc. No. 730 (AIP, New York, 2004), p. 139.
[11] V. Recoules, P. Renaudin, J. Clerouin, P. Noiret, and G. Zerah, Phys. Rev. E **66**, 056412 (2002).
[12] V. Recoules and J. P. Crocombette, Phys. Rev. B **72**, 104202 (2005).
[13] S. Mazevet, M. P. Desjarlais, L. A. Collins, J. D. Kress, and N. H. Magee, Phys. Rev. E **71**, 016409 (2005).
[14] L. X. Benedict, J. E. Klepeis, and F. H. Streitz, Phys. Rev. B **71**, 064103 (2005).
[15] S. Mazevet and G. Zerah, Phys. Rev. Lett. **101**, 155001 (2008).
[16] X. Gonze, J. M. Beuken, R. Caracas, F. Detraux, M. Fuchs, G.-M. Rignanese, L. Sindic, M. Verstraete, G. Zerah, F. Jollet, M. Torrent, A. Roy, M. Mikami, Ph. Ghosez, J.-Y. Raty, and D. C. Allan, Comput. Mater. Sci. **25**, 478 (2002).
[17] F. Bottin, S. Leroux, A. Knyazev, and G. Zerah, Comput. Mater. Sci. **42**, 329 (2008).
[18] P. E. Blöchl, Phys. Rev. B **41**, 5414 (1990).
[19] M. Torrent, F. Jollet, F. Bottin, and G. Zerah, Comput. Mater. Sci. **42**, 337 (2008).
[20] J. P. Perdew, K. Burke, and M. Ernzerhof, Phys. Rev. Lett. **77**, 3865 (1996).
[21] N. A. W. Holzwarth, A. R. Tackett, and G. E. Matthews, Comput. Phys. Commun. **135**, 329 (2001).
[22] J. L. F. Da Silva, Phys. Rev. B **71**, 195416 (2005).
[23] M. Taillefumier, D. Cabaret, A. M. Flank, and F. Mauri, Phys. Rev. B **66**, 195107 (2002).
[24] C. J. Pickard, Ph.D. thesis, University of Cambridge, 1997.
[25] F. Dorchies, M. Harmand, D. Descamp, C. Fourment, S. Hulin, S. Petit, O. Peyrusse, and J. J. Santos, Appl. Phys. Lett. **93**, 121113 (2008).
[26] S. P. Gao, C. J. Pickard, M. C. Payne, J. Zhu, and J. Yuan, Phys. Rev. B **77**, 115122 (2008).
[27] G. Onida, L. Reining, and A. Rubio, Rev. Mod. Phys. **74**, 601 (2002).
[28] A. Kiejna, G. Kresse, J. Rogal, A. De Sarkar, K. Reuter, and M. Scheffler, Phys. Rev. B **73**, 035404 (2006).
[29] M. Marsman and G. Kresse, J. Chem. Phys. **125**, 104101 (2006).
[30] W. Johnson, C. Guet, and G. F. Bertsch, J. Quant. Spectrosc. Radiat. Transf. **99**, 327 (2006).
[31] S. P. Lyon and J. D. Johnson, Los Alamos Report No. LA-UR-92–3407, 1992.
[32] P. M. Celliers, G. W. Collins, D. G. Hicks, and J. H. Eggert, J. Appl. Phys. **98**, 113529 (2005).